# Controller-Induced Parasitic Torque Ripples in a PM Synchronous Motor

Shaotang Chen, *Senior Member, IEEE*, Chandra Namuduri, and Sayeed Mir

***Abstract*—Permanent magnet (PM) synchronous machines with a sinusoidal back electromotive force are ideally capable of torque-ripple-free operation. However, parasitic torque ripples can still be induced from motor design and controller implementation. This paper focuses on a systematic analysis of possible sources of torque ripple in a PM synchronous machine drive resulting from limitations in the motor controller. It takes into account the effects of finite encoder resolution, controller CPU word length, current sensing errors, and inverter pulsewidth-modulation switching. Approaches for analyzing and calculating torque ripple from each of those sources have been developed. Characteristics of the various parasitic torque ripples are discussed. Experimental and simulation data to verify important results are also presented.**

***Index Terms*—CPU word length, current control, current sensing accuracy, digital control, digitization error, encoder resolution, field orientation, influence of controller, parasitic torque ripple, PM synchronous machine, permanent magnet motor, pulsewidth modulation, PWM inverter, torque ripples.**

## I. Introduction

In the search for a torque-ripple-free permanent magnet (PM) machine drive, a PM machine with a sinusoidal back electromotive force (EMF) is favored over one with a trapezoidal back EMF. When supplied with a sinusoidal current, the sinusoidal PM machine is ideally capable of producing a constant torque with zero torque ripple. Theoretically, a PM machine should also be able to produce zero torque ripple with a trapezoidal EMF if a rectangular current is provided. However, since a rectangular current implies an infinite current control bandwidth or an infinite $di/dt$, generation of such a current profile is obviously impractical due to existence of machine inductance. The resulting nonrectangular currents produce considerable torque ripple known as commutation torque ripple. Conversely, a sinusoidal current profile requires only a finite current control bandwidth proportional to the motor speed. It is feasible to produce such a current waveform, especially at low motor speeds. Thus, a true torque-ripple-free PM machine drive must be based on the sinusoidal PM synchronous machine.

Paper IPCSD 02–031, presented at the 2000 Industry Applications Society Annual Meeting, Rome, Italy, October 8–October 12, and approved for publication in the IEEE Transactions on Industry Applications by the Electric Machines Committee. Manuscript submitted for review May 1, 2001 and released for publication June 7, 2002.

S. Chen is with Delphi Research Laboratories, Shelby Township, MI 48315 USA.

C. Namuduri is with the Research and Development Center, General Motors, Warren, MI USA 48090 (e-mail: Chandra.S.Namuduri@gm.com).

S. Mir is with Delphi Saginaw Steering Systems, Saginaw, MI 48601 USA.

Publisher Item Identifier 10.1109/TIA.2002.803000.

However, parasitic torque ripples still exist, even in a sinusoidal PM motor drive, due to limitations in machine design and controller implementation. From a machine design standpoint, a sinusoidal back EMF requires a sinusoidal distribution of magnet flux and windings. Due to limitations in magnetization and available slots for a winding distribution, harmonics in the back EMF and, thus, their associated torque ripples, are unavoidable. Also, the interaction between the magnets and slots of a slotted machine produces a nonuniform magnetic force, resulting in the so-called cogging torque. In addition, torque ripples can still be produced by magnetic asymmetry such as that due to rotor eccentricity. Analyses and methods for overcoming those problems related to machine design have gained considerable importance in the literature [1], [2]. For applications requiring an ultra-low ripple torque, a practical solution in machine design seems to use air-gap windings to virtually eliminate the cogging torque, improve the sinusoidal winding distribution, and reduce the sensitivity to eccentricity owing to a large air gap.

From a controller design standpoint, there still exist tremendous challenges in providing a pure sinusoidal current waveform to the machine. In particular, the motor controller has to be built using either an analog or digital circuitry. Due to advantages in flexibility and implementation offered by a digital control system, almost all motor controllers built today are in digital format using a digital signal processor (DSP) or microcontroller. The drive for a low-cost implementation has always prompted the use of microprocessors with a minimum word length, encoders with the lowest number of pulses per revolution, and current sensors with the lowest possible accuracy. The above controller design considerations have imposed considerable limitations on the various performance factors of a motor drive system. They have been found to contribute to torque ripples with levels comparable to or even higher than those associated with the machine design limitations. It is, therefore, desirable to investigate the effects of the controller parameters on the torque-ripple performance of PM synchronous machines.

Historically, very few publications have addressed the influence of controller design parameters on machine torque-ripple performance. In [3], the effect of word length of a digital controller on pulsewidth-modulation (PWM) harmonics is examined, though it is limited only to PWM waveform generation. Although [4] considers the effect of digitization in general, it fails to recognize some of the more important effects such as those due to finite encoder resolution and accumulation errors caused by a finite CPU word length. The impact of current sensor inaccuracy on torque ripple has also been recognized in [5], but only for induction machine drives. Therefore, there is still a lack of a systematic analysis of effects of controller limitations on PM synchronous motor drive performance.

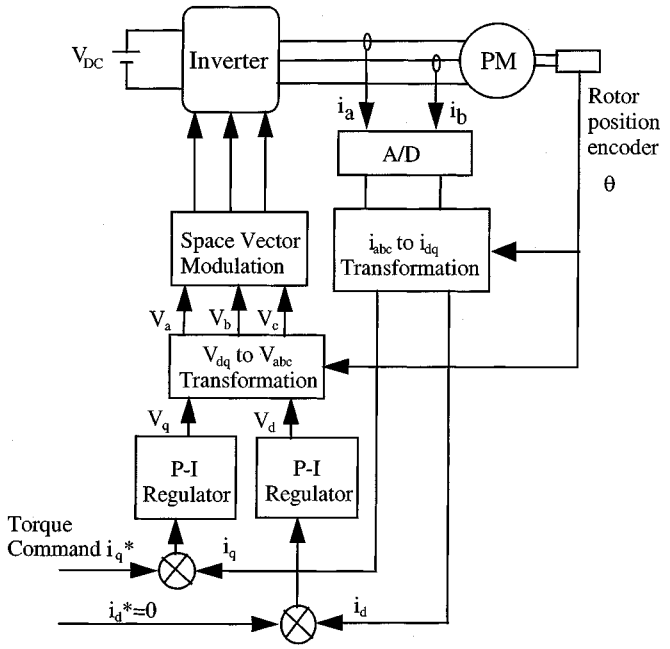


Fig. 1. Current vector controller for a PM machine drive.

This paper provides a systematic analysis of major possible sources of parasitic torque ripples associated with a digital controller in a PM synchronous machine. It is aimed at quantifying the effect of each of the major controller design parameters on torque-ripple performance. The controller parameters investigated include available encoder resolution, CPU word length, current sensor accuracy, etc. In Section II, all major contributors to parasitic torque ripples in a PM synchronous motor drive will be summarized. Their effects and quantification are then presented in Section III.

## II. Sources of Parasitic Torque Ripples Associated With a Digital Controller

A standard synchronous PM motor drive with a digital current vector/field orientation controller has a block diagram, as shown in Fig. 1. Torque-ripple-free operation of an ideal PM synchronous machine with a pure sinusoidal back EMF and zero-cogging torque requires an ideal sinusoidal current synchronized with the back EMF waveform. These currents are supplied by the machine controller, which includes the control logic and power converter. Any controller parameter that causes the motor currents to deviate from the synchronized sinusoidal waveforms will constitute a source of torque ripple. Depending on the digital controller configuration, the major sources of parasitic torque ripples are generally related to the following controller limitations.

### A. Position Sensor Limitation

This is mainly due to a finite resolution in position information provided by a digital shaft encoder. As an encoder is an expensive component, it is desirable to reduce its cost by using the lowest possible resolution. Some operating requirements may also require the use of specific types of encoders, such as the Hall-effect type, which can only provide a relatively low resolution. Thus, this limitation can easily become the dominant source of quantization error in a PM drive system and often produces a much larger torque ripple than that caused by other quantization errors such as those related to a finite CPU word length and A/D converter bit resolution.

TABLE I
PM Synchronous Motor Parameters

| | |
|---|---|
| Pole Number | $N_p = 4$ |
| Input DC Voltage | $V_{dc} = 12$ V |
| Effective Phase Resistance | $R = 55$ mΩ |
| Effective Phase Inductance | $L_s = 38.5$ μH |
| Maximum Reactance | $X_s=\omega_e L_s = 22.5$ mΩ |
| EMF Constant | $K_e = 0.023$ V/(rad/s) |

### B. Computational Error

This is mainly due to finite CPU data bits/word length. The CPU word length will cause discretization errors in control variables and parameters. Any calculated result has to be truncated to fit into the available word length and must carry a truncation error. In addition, calculations in control algorithms will force the above errors to propagate and accumulate. The end result is to produce deviations of control voltages or currents from the ideal sinusoidal values resulting in torque ripple.

### C. Imperfect Current Sensing

An ideal current sensor simply does not exist, and all current sensors inherently have offset and gain mismatch inaccuracies. Since the field orientation control relies on current feedback, any inaccuracy in current sensing will directly impact torque-ripple performance. A quantitative analysis of this effect will undoubtedly provide great benefits to the drive system design.

### D. PWM Switching

This is due to limitations in using a PWM inverter to generate a sinusoidal current waveform. The current produced by PWM switching has a high-frequency ripple associated with the PWM switching frequency. The high-frequency ripple current interacts with the motor back EMF and produces a high-frequency torque ripple. Also, an unsynchronized PWM frequency and fundamental frequency components can lead to a beat frequency harmonics in torque, which may become appreciable with a relatively low ratio between the switching and fundamental frequencies.

It is important to point out that this paper will not address the effect of control loop process time on torque ripple. A control loop process time is the time a CPU takes to update a control variable. A large loop process time can have a considerable influence on torque ripple. However, due to other more stringent performance requirements, such as system dynamic response and so on, the loop time is usually designed to be short enough and, therefore, rarely become an issue for torque ripple.

Section III will focus on a detailed analysis of the effect of the above limitations on the torque-ripple performance of a three-phase PM synchronous motor.

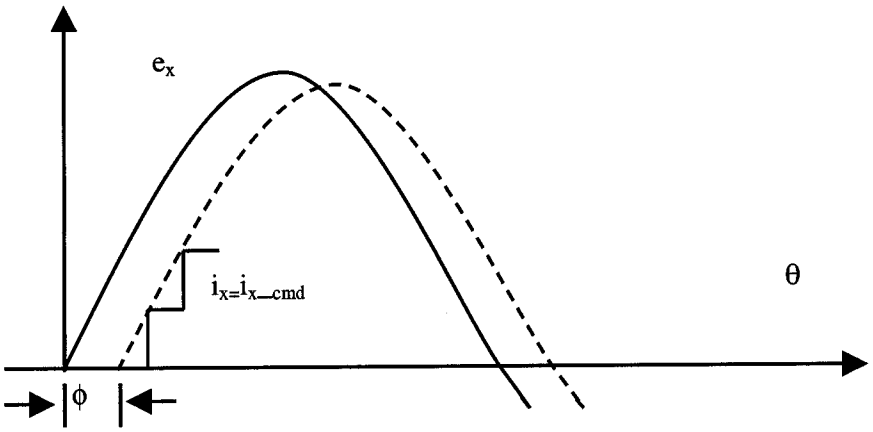


Fig. 2. Influence of encoder resolution.

## III. Torque-Ripple Analysis

To simplify the analysis, effects of only one controller parameter will be considered at a time. The quantification and experimentation will be based on a three-phase sinusoidal PM machine with air-gap windings, which has almost zero cogging torque ripple. The motor parameters are listed in Table I.

### A. Effect of Finite Encoder Resolution

The discrete position information provided by an encoder with a finite resolution will cause discretization errors in the controller through the $d$–$q$ transformations, as can be seen from Fig. 1. Analysis of its influence through the $d$–$q$ model itself can be very difficult and daunting [4]. This problem can be circumvented elegantly by converting the system representation back to the stationary stator frame. In the stationary frame, the encoder information will appear only on the sinusoidal current command and it will cause a discrete current command $i_{x\_\mathrm{cmd}}$ ($x = a$, $b$, or $c$), as shown in Fig. 2. Since a high-performance current regulator exists for each of the phases, the actual motor phase current $i_x$ will be forced to follow the same staircase shape of the current command.

Assume that $\theta_{\mathrm{res}}$ represents the encoder resolution in electric degrees per count, $\theta$ represents the actual rotor position, and $\theta_d$ represents the corresponding discrete rotor position provided by an encoder. Denote $\gamma = \theta - \theta_d$ with $0 \le \gamma \le \theta_{\mathrm{res}}$. For any given position $\theta$, the back EMFs of a three-phase motor can be expressed as

$$e_a = E\sin(\theta_d + \gamma) \tag{1}$$

$$e_b = E\sin\left(\theta_d + \gamma - \frac{2\pi}{3}\right) \tag{2}$$

$$e_c = E\sin\left(\theta_d + \gamma + \frac{2\pi}{3}\right). \tag{3}$$

The motor current is assumed to lag the motor back EMF by an angle $\phi$, which is a constant parameter set by the controller. Correspondingly, the motor phase currents will be

$$i_a = I\sin(\theta_d - \phi) \tag{4}$$

$$i_b = I\sin\left(\theta_d - \phi - \frac{2\pi}{3}\right) \tag{5}$$

$$i_c = I\sin\left(\theta_d - \phi + \frac{2\pi}{3}\right). \tag{6}$$

The torque equation within each encoder step or for $0 \le \gamma \le \theta_{\mathrm{res}}$ is

$$\begin{aligned} T &= \frac{1}{\omega_m}\sum_{i}^{a,b,c} e_i i_i \\ &= \frac{EI}{\omega_m}\sum_{i=1}^{3}\sin\left[\theta_d + \gamma - (i-1)\frac{2\pi}{3}\right] \\ &\quad \cdot \sin\left[\theta_d - \phi - (i-1)\frac{2\pi}{3}\right] \\ &= \frac{3}{2}\frac{EI}{\omega_m}\cos(\gamma + \phi). \end{aligned} \tag{7}$$

Since the motor torque depends only on the angle $\gamma$, it has a period equal to the encoder resolution, i.e.,

$$T(\gamma + n\theta_{\mathrm{res}}) = T(\gamma), \qquad \text{for } n = 1, 2, 3, \ldots. \tag{8}$$

It can be seen that the torque will have a periodical ripple component with a frequency equal to that of the encoder position counting pulse.

Based on the above torque equations (7) and (8), the per unit peak-to-peak torque ripple can also be calculated as

$$T_{r,\,\mathrm{pk-pk}}(\gamma) = \max\big(\cos(\gamma+\phi)\big) - \min\big(\cos(\gamma+\phi)\big), \quad 0 \le \gamma \le \theta_{\mathrm{res}}. \tag{9}$$

Therefore, the relationship between the worst-case peak-to-peak torque ripple and encoder resolution can be plotted as shown in Fig. 3(a). A measurement of the motor torque waveform versus rotor position was performed at zero speed. With an encoder resolution of ten electric degrees, the torque ripple is plotted in Fig. 3(b). It shows a 4% peak-to-peak torque ripple, which is in good agreement with the prediction of 4.5% from Fig. 3(a).

### B. Effect of Finite CPU Word Length

The CPU word length affects the accuracy of variables stored in the computer and produces the so-called quantization error. The calculations in control algorithms by the CPU also produce truncation and propagation errors. Those errors will accumulate on the calculated voltage information to be sent to the inverter.

To focus on an analysis of these types of errors, the following derivation assumes no A/D digitization error in the current feedback and no additional voltage error caused by digitization

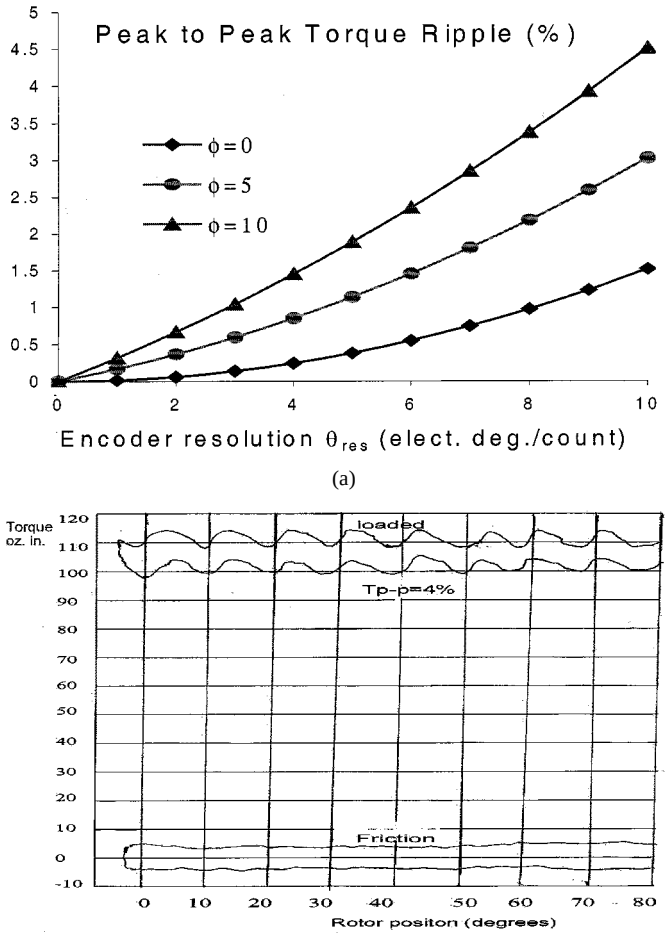


Fig. 3. Torque ripple due to a finite encoder resolution.

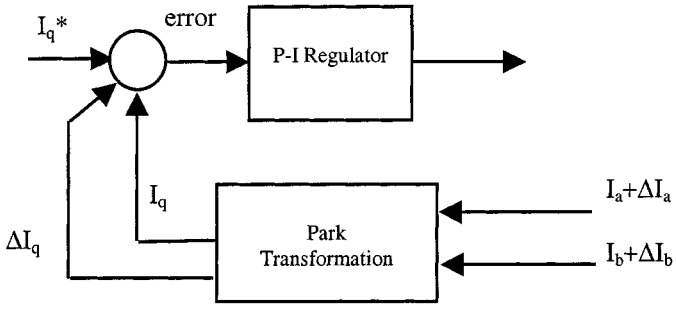


Fig. 4. Error propagation in a $q$-axis current control algorithm.

effect of inverter. With such assumptions, the errors and their propagation paths due to CPU word length can be depicted as shown in Fig. 4.

As the $q$-component of current directly images the electromagnetic torque of the motor while the $d$-component is kept zero, the torque is primarily affected by the resolution of the $q$-component of current. Assuming an $n$-bit fixed-point processor and neglecting other errors, all variables input directly to the CPU will have a maximum truncation error equal to $1/2^{n-1}$ of its maximum value. To simplify the analysis, it is assumed that all CPU data is stored in the per-unit values and no other scaling factors for control variables exist. Also, to facilitate the analysis, the following notation is introduced: a variable starting with a capitalized letter will denote a per-unit value, such as $I_a$, and the same variable starting with a lower case letter, e.g., $i_a$, will be the corresponding nonscaled or actual value. The value stored by CPU will be denoted using a superscript $d$. With this notation, for a phase current $i_a$, the per-unit value will be represented by $I_a = i_a/I_{\max}$ and the discrete CPU value is $I_a^d$. In an $n$-bit CPU, $I_a^d = I_a + \Delta I_a$, where $|\Delta I_a| < 1/2^{n-1}$ is the truncation error.

As the $d$–$q$ current calculation in the CPU is given by the following equations:

$$I_q^d = \frac{2}{3}\left[I_a^d\cos^d(\theta) + I_b^d\cos^d\left(\theta - \frac{2\pi}{3}\right) + I_c^d\cos^d\left(\theta + \frac{2\pi}{3}\right)\right] \tag{10}$$

$$I_d^d = \frac{2}{3}\left[I_a^d\sin^d(\theta) + I_b^d\sin^d\left(\theta - \frac{2\pi}{3}\right) + I_c^d\sin^d\left(\theta + \frac{2\pi}{3}\right)\right] \tag{11}$$

substituting the nontruncated or accurate values into the $Iq$ equation will give

$$\begin{aligned} I_q^d = \frac{2}{3}\Bigg\{&\left[I_a\cos\theta + I_b\cos\left(\theta - \frac{2\pi}{3}\right) + I_c\cos\left(\theta + \frac{2\pi}{3}\right)\right] \\ &+ \left[\Delta I_a\cos\theta + \Delta I_b\cos\left(\theta - \frac{2\pi}{3}\right) + \Delta I_c\cos\left(\theta + \frac{2\pi}{3}\right)\right] \\ &- \left[I_a\Delta\cos\theta + I_b\Delta\cos\left(\theta - \frac{2\pi}{3}\right) + I_c\Delta\cos\left(\theta + \frac{2\pi}{3}\right)\right]\Bigg\} + o^2(\Delta) \\ = I_q + \Delta I_q. \end{aligned} \tag{12}$$

Since all the $\Delta$ errors in above equation are less than or equal to $1/2^{n-1}$, by neglecting the second-order terms, the accumulation error contained in $I_q^d$ is

$$|\Delta I_q|_{\text{accum}} \le \frac{2}{3}\frac{6}{2^{n-1}} = \frac{4}{2^{n-1}}. \tag{13}$$

Adding a truncation error of $1/2^{n-1}$ to the calculated result yields a total error

$$|\Delta I_q|_{\text{total}} \le \frac{5}{2^{n-1}}. \tag{14}$$

This error of $I_q$ is fed as an input to the $q$-axis current regulator, as shown in Fig. 4. Assuming a reasonable current regulator design, this will force the actual motor current to produce an error equal to $I_{\max}\cdot\Delta I_q$. As the calculation error is a random noise, this current error can be both positive and negative, and the torque output will fluctuate up and down from its nominal value, directly contributing to the torque ripple. Therefore, the per-unit torque ripple will be equal to the absolute value of the $I_q$ current error and the peak-to-peak torque ripple is

$$T_r = \frac{10}{2^{n-1}}.$$

A plot of the torque ripple versus CPU word length is shown in Fig. 5.

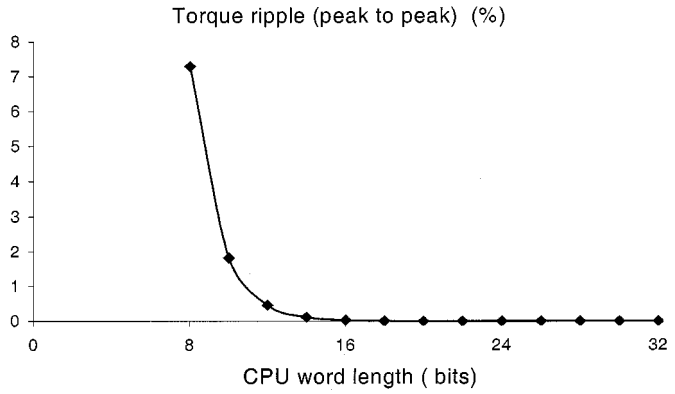


Fig. 5. Torque ripple versus CPU word length.

### C. Effect of Current Sensor Inaccuracy

A current sensing circuit used for a PM motor drive has the following two sources of errors: dc offset and gain mismatch. The dc offset is a dc component superimposed on the accurate phase-current measurement. It can be caused by: 1) the sensor; 2) the processing amplifier; or 3) both. The magnetic hysteresis in a Hall-effect sensor is usually the main contributor for a dc offset. The gain mismatch is due to differences in amplifying gains of the corresponding current-processing amplifiers. Their effects on torque ripple can be analyzed as follows.

*DC Offset:* Assume that the three-phase PM machine has a neutral connection and only two (2) phase-current sensors are used for current feedback. If the two phase-current sensing circuits have dc offsets given by

$$i_a = I[\sin\theta + \Delta_a] \tag{15}$$

$$i_b = I\left[\sin\left(\theta - \frac{2\pi}{3}\right) + \Delta_b\right] \tag{16}$$

where $\Delta_a$ and $\Delta_b$ are the per-unit dc-offset values of the two phase-current sensors, and $I$ is the actual current amplitude. The phase "$c$" current $i_c$ is usually calculated by the controller using the following:

$$i_c = -(i_a + i_b) = I\left[\sin\left(\theta + \frac{2\pi}{3}\right) - (\Delta_a + \Delta_b)\right]. \tag{17}$$

Based on the assumption of ideal current regulation, the motor torque will be

$$\begin{aligned} T &= \frac{1}{\omega_m}\sum_{i}^{a,b,c} e_i i_i \\ &= \frac{EI}{\omega_m}\left\{\frac{3}{2} + \Delta_a\left[\sin\theta - \sin\left(\theta + \frac{2\pi}{3}\right)\right]\right. \\ &\qquad \left. + \Delta_b\left[\sin\left(\theta - \frac{2\pi}{3}\right) - \sin\left(\theta + \frac{2\pi}{3}\right)\right]\right\} \\ &= \frac{EI}{\omega_m}\left\{\frac{3}{2} + \sqrt{3}\left[\Delta_a\cos\left(\theta - \frac{2\pi}{3}\right) - \Delta_b\cos\theta\right]\right\}. \end{aligned} \tag{18}$$

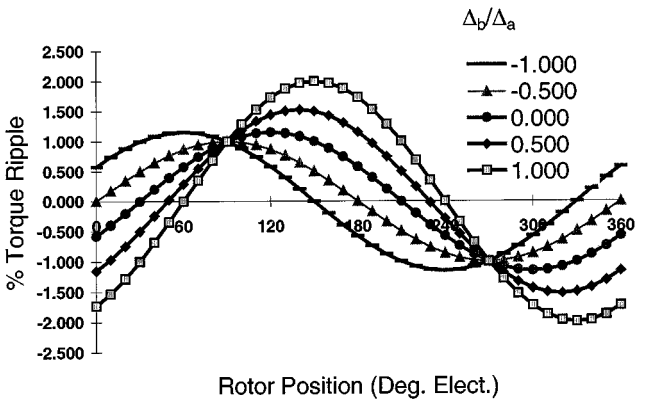


(a)

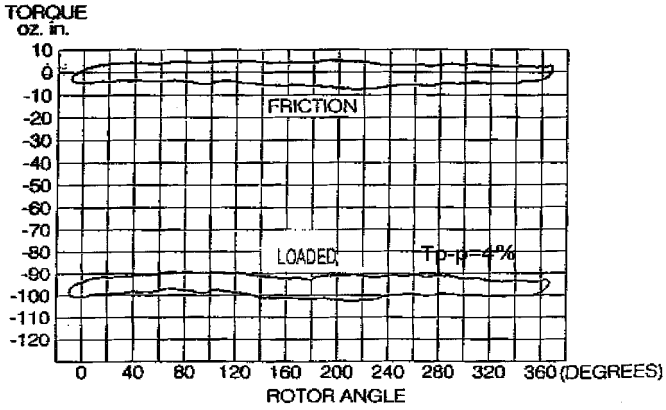


(b)

Fig. 6. Torque ripple due to current sensor dc-offset errors.

From the above torque equation, it can be shown that the peak-to-peak torque ripple will have a fundamental frequency component given in per unit as

$$T_r = \frac{2}{\sqrt{3}}\left[\Delta_a\cos\left(\theta - \frac{2\pi}{3}\right) - \Delta_b\cos\theta\right]. \tag{19}$$

Given a 1% dc offset in phase "$a$," as the dc offset in phase "$b$" varies, a series of the torque-ripple waveforms are plotted in Fig. 6(a). It can be seen that the zero crossing point or the phase shift of torque-ripple waveform changes with the offset ratio between phases "$a$" and "$b$." Due to this characteristic, it is very difficult to compensate this type of torque ripple.

Assuming that the maximum offset for all current sensors is $\Delta$, the worst-case ripple torque will occur when $\Delta_a = \Delta_b = \Delta$ and is given by

$$T_r = 2\Delta\sin\left(\theta - \frac{\pi}{3}\right), \qquad 0 < \theta < 2\pi. \tag{20}$$

This indicates that a torque ripple at the fundamental frequency will be produced by a dc offset. Under worst conditions, a 1% dc offset can result in a 4% peak-to-peak ripple torque. An experimental verification was obtained by introducing intentionally a 1% dc offset in both phase-current measurement. The same torque-ripple characteristics, as predicted in Fig. 6(a),

are observed in the measured torque-ripple waveform shown in Fig. 6(b).

*Gain Mismatch:* Gain mismatch means that the current gain of one phase is different from that of the other phase. If the two phase currents have a gain mismatch, as given by

$$i_a = I(1+k_1)\sin\theta \tag{21}$$

$$i_b = I(1+k_2)\sin\left(\theta - \frac{2\pi}{3}\right) \tag{22}$$

where $k_1$ and $k_2$ is the per-unit errors in gains of the two sensor circuits, respectively, the calculated phase $c$ current will be

$$\begin{aligned} i_c &= -(i_a + i_b) \\ &= I\left[\sin\left(\theta + \frac{2\pi}{3}\right) - k_1\sin\theta - k_2\sin\left(\theta - \frac{2\pi}{3}\right)\right]. \end{aligned} \tag{23}$$

Under the assumption of ideal current regulation, the motor torque is

$$\begin{aligned} T &= \frac{1}{\omega_m}\sum_{i}^{a,b,c} e_i i_i \\ &= \frac{EI}{\omega_m}\left\{\frac{3}{2} + k_1\sin\theta\left[\sin\theta - \sin\left(\theta + \frac{2\pi}{3}\right)\right]\right. \\ &\qquad + k_2\sin\left(\theta - \frac{2\pi}{3}\right) \\ &\qquad \left.\cdot\left[\sin\left(\theta - \frac{2\pi}{3}\right) - \sin\left(\theta + \frac{2\pi}{3}\right)\right]\right\} \\ &= \frac{EI}{\omega_m}\left[\frac{3}{2} + \frac{3}{4}(k_1+k_2) + \frac{\sqrt{3}}{2}(k_1-k_2)\sin\left(2\theta - \frac{2\pi}{3}\right)\right]. \end{aligned} \tag{24}$$

It can be shown that the torque ripple will have a component at twice the fundamental frequency given in per unit as

$$T_r = \frac{2}{\sqrt{3}}\frac{k_1 - k_2}{2 + k_1 + k_2}\sin\left(2\theta - \frac{2\pi}{3}\right), \qquad \text{for } k_1 \neq k_2; \quad 0 < \theta < 2\pi. \tag{25}$$

The worst-case torque ripple happens with $k_1 = -k_2 = \Delta_k$ and the peak-to-peak ripple is calculated as

$$T_r = \frac{4}{\sqrt{3}}\Delta_k \tag{26}$$

i.e., for 1% of gain mismatch, the worst case is a 2.31% of peak-to-peak torque ripple at twice the fundamental frequency.

The torque ripple due to a gain mismatch is plotted as shown in Fig. 7(a). An experimental measurement of the effect of introducing approximately 2% gain mismatch is shown in Fig. 7(b).

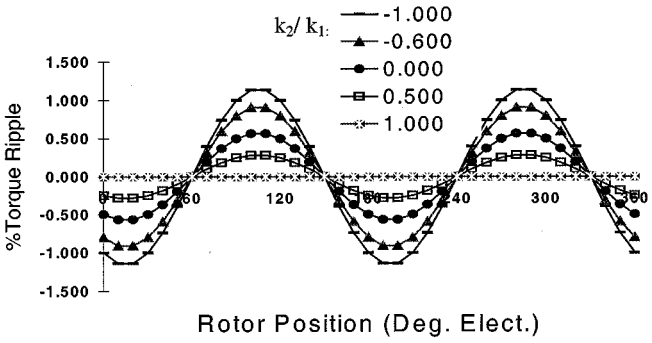


(a)

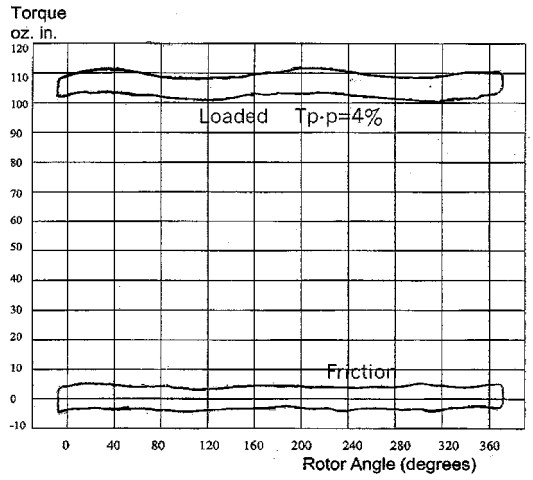


(b)

Fig. 7. Torque ripple due to current sensor gain mismatch.

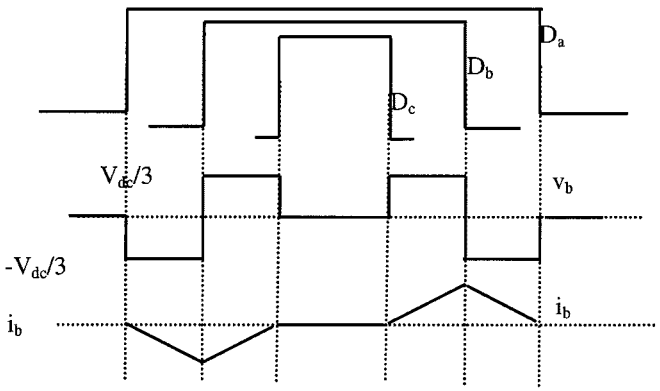


Fig. 8. Inverter swiching effect on motor phase voltages and currents.

### D. Effect of PWM Inverter

*Finite Pulsewidth Resolution:* The pulsewidth is digitally adjusted in a digital controller. The minimum increment/decrement step is determined by the number of bits of the pulsewidth register. This effect is to produce a hysteresis band on the generated voltage. This hysteresis band is equal to $1/2^{n-1}V$ with $V$ equal to the ideal motor voltage and $n$ representing the pulsewidth resolution. The resulting torque fluctuation can be calculated based on the following torque equation:

$$T = 3 \cdot K_e \cdot \frac{(V\cos\delta - K_e\omega_m)R + X_s V\sin\delta}{R^2 + X_s^2} \tag{27}$$

where $V$ is the rms phase voltage, $\omega_m$ is the motor speed, and $\delta$ is the angle between the voltage and back EMF phasors. By substituting $\Delta V/V = 1/2^{n-1}$ in the above equation, the torque ripple can be calculated as

$$T_r = \frac{\Delta T}{T} = \frac{1}{2^{n-1}}\frac{\cos\delta\cdot R + X_s\cdot\sin\delta}{\left(\cos\delta - \dfrac{E}{V}\right)R + X_s\cdot\sin\delta}. \tag{28}$$

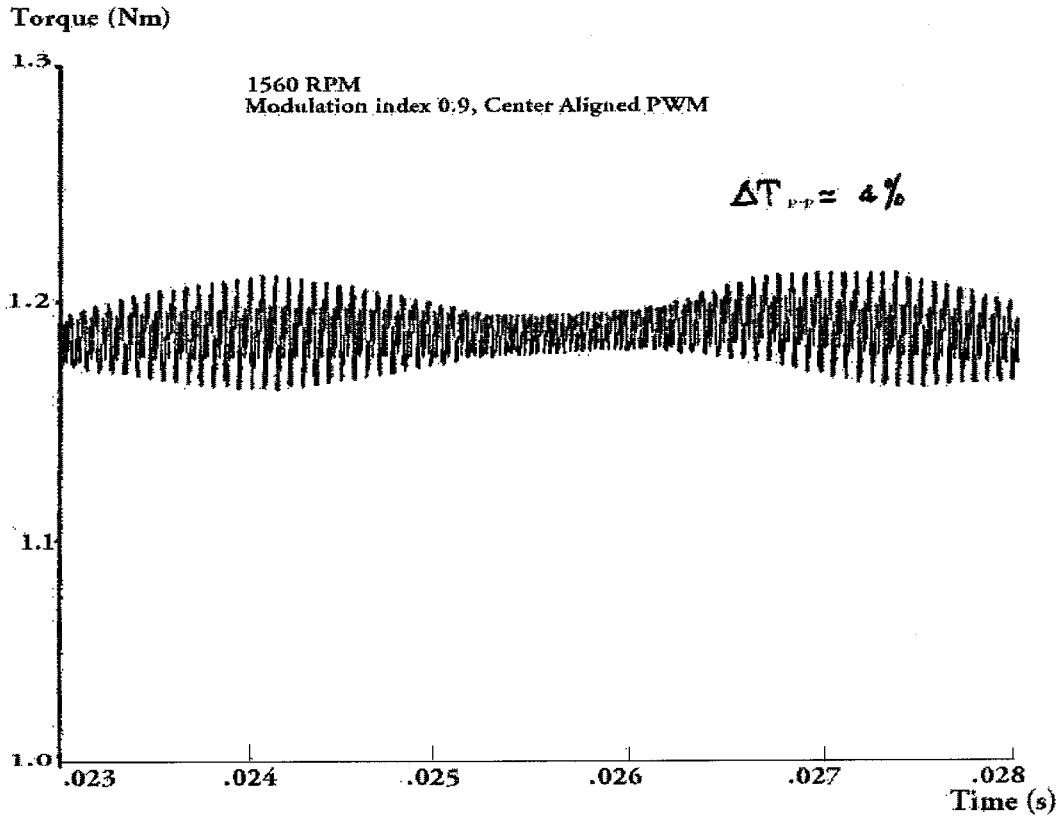


Fig. 9. Torque ripple due to PWM controlled current.

*PWM Switching Effect:* Another type of torque ripple is caused by the PWM switching effect that produces a current ripple at the switching frequency. This ripple is caused as the phase may see both positive and negative voltage in order to get a desired average during one PWM cycle. Fig. 8 shows the duty cycles of three phases near the zero crossing of phase "$b$" voltage. Phase "$b$" sees $V_{\rm dc}/3$ and $-V_{\rm dc}/3$ for equal duration resulting in zero average voltage across the phase. Although the average current is zero, there is a change in current during the positive and negative periods of the voltage resulting in a current ripple. The change in phase current during the PWM interval is given by

$$\frac{di}{dt} = \frac{1}{L_s}(V - iR - E). \tag{29}$$

Assuming linear change, we can say

$$\Delta i = \Delta T_{\rm on}\frac{1}{L_s}(V - iR - E) \tag{30}$$

where $\Delta T_{\rm on}$ is the on-time during the PWM cycle, which causes current ripple and is given by

$$\Delta T_{\rm on} = 0.5M\left[\sin\left(\theta - \frac{2\pi}{3}\right) - \sin\theta\right]T_s \tag{31}$$

where $M = V/V_{\rm dc}$ is the modulation voltage, $T_s$ is the PWM time period, and $\theta$ is the angle from zero crossing of the phase voltage and varies from 0° to +30°.

The above equations show that the current ripple is affected by the rotor position angle, current amplitude, and back EMF voltage. The ripple is highest at low current, high voltages, and low speeds. Also, the amplitude of this ripple changes as a function of motor position. For a constant current and back EMF, the ripple is highest at the zero crossing of the voltage and decreases on both sides for 30° where the effect becomes zero. Since there are six zero crossing points, the frequency of this ripple profile is, therefore, six times the fundamental frequency.

Assuming no phase advancing and current vector being in-phase with back EMF, the percentage of torque ripple is the same as that of the current ripple. Depending on the PWM scheme, the amplitude of the current ripple and, thus, the torque ripple, can vary considerably. For a space vector modulation, the torque ripple is plotted as shown in Fig. 9.

*Dead-Time:* The dead time is inserted between complementary switching of upper and lower switches in a phase leg to avoid any shoot through. This causes a loss of a portion of the duty cycle and, thus, the voltage applied to the phases. This effect becomes more pronounced near the zero crossing of the current. During the dead time, the current can only flow through the diodes of the inverter. Regardless of the current direction, the magnitude of current decreases toward zero and clamps there during the rest of the dead time as the reverse voltage of the diodes blocks the current flow. Fig. 10 shows the current waveform with the effects of dead time. The currents become very distorted when the magnitude of current is near zero. Moreover, the $a$ phase current is also distorted when the $b$ and $c$ phase currents are near zero (not shown in Fig. 10). As there are six zero crossings per electrical cycle in a three-phase PM machine, the

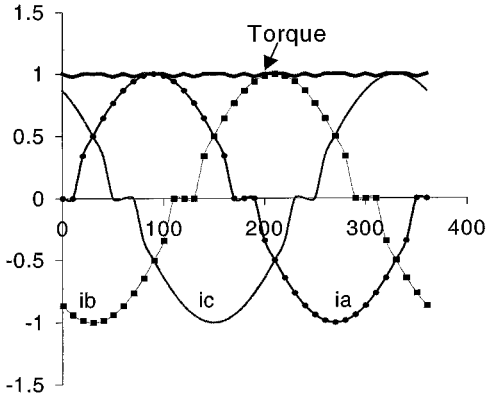


Fig. 10. Torque ripple due to inverter dead time.

torque ripple produced by such current waveform will have a sixth harmonic frequency as shown in Fig. 10.

Considering the zero crossing of the phase "$a$" current, the line-to-neutral voltage of the phases during the zero clamping of the $a$ phase current is given by [6]

$$v_{an} = e_{an} \tag{32}$$

$$v_{bn} = \frac{v_{bo} - v_{co} - e_{an}}{2} \tag{33}$$

$$v_{cn} = \frac{v_{co} - v_{bo} - e_{an}}{2} \tag{34}$$

where $e_{an}$ is the back EMF across $a$ phase and $v_{bo}$ and $v_{co}$ is the voltage relative to negative dc bus at the terminals of phase "$b$" and "$c$," respectively. The voltages can be represented in stationary reference frame as

$$v_q = v_{an} = e_{an} \tag{35}$$

$$v_d = \frac{v_{cn} - v_{bn}}{\sqrt{3}} \tag{36}$$

which shows that near the zero current crossing of $a$ phase, only the stationary reference frame $q$-axis voltage is distorted. Thus, the distortion in voltage in the stationary reference frame is given by the following vectors:

$$\Delta v_q = v_{an}^* \text{ and } \Delta v_d = 0 \tag{37}$$

where $v_{an}^*$ is the reference phase voltage (or command voltage) at the current zero crossing point. The reference voltage is dependent upon the direction of current [6] and is given as $v_{an}^* = (2/3)V_{\rm dc}$ for negative currents and $v_{an}^* = 0$ for positive currents. With the $v_{an}^*$ value determined, the torque ripple due to this voltage distortion can be determined from the resulting current distortion during the dead time. The current ripple or distortion can be calculated based on the $q$-axes equation as

$$\Delta i_q \approx \frac{\Delta v_q}{L_s} T_d = \frac{v_{an}^*}{L_s} T_d \tag{38}$$

where the motor resistance voltage drop is neglected and $T_d$ is the dead-time duration. As $\Delta i_q$ contributes to the torque component, the percentage of torque ripple will be proportional to the relative value of $\Delta i_q$ versus the nominal motor phase-current amplitude. It is calculated that for a 2-$\mu$s dead time, the torque ripple will be 2% peak-to-peak.

## IV. Conclusions

An analysis of parasitic torque ripples caused by the motor controller of a PM synchronous motor drive with a sinusoidal back EMF has been presented. It has been shown that the encoder resolution, CPU word length, current sensing errors, and inverter PWM switching all have a considerable effect on the torque-ripple performance. Methods and formulas for calculating the torque ripples associated with each of these controller parameters are derived. The developed torque-ripple analysis should be useful to assist in the design and selection of optimal controller parameters for meeting given torque-ripple requirements at a minimum cost. In addition, the approaches developed for motor torque-ripple calculations can be applied to other type of motor drives including induction and switched reluctance motor drives.

## References

[1] D. Staton, R. P. Deodhar, W. L. Soong, and T. J. E. Miller, "Torque prediction using the flux-MMF diagram in AC, DC and reluctance motors," *IEEE Trans. Ind. Applicat.*, vol. 32, pp. 180–188, Jan./Feb. 1996.

[2] T. Sebastian and V. Gangla, "Analysis of induced EMF waveforms and torque ripple in a brushless permanent magnet machine," *IEEE Trans. Ind. Applicat.*, vol. 32, pp. 195–200, Jan./Feb. 1996.

[3] D. A. Grant, M. Stevens, and J. A. Houldsworth, "The effect of word length on harmonic content of microprocessor-based PWM waveform generators," *IEEE Trans. Ind. Applicat.*, vol. IA-21, pp. 218–225, Jan./Feb. 1985.

[4] D. Grenier, F. Labrique, E. Matagne, and H. Buyse, "Discretization effects on the control of voltage-source inverter-fed permanent-magnet synchronous motor drives," *Electromotion*, no. 4, pp. 155–163, 1997.

[5] D.-W. Chung and S.-K. Sul, "Analysis and compensation of current measurement error in vector controlled AC motor drives," *IEEE Trans. Ind. Applicat.*, vol. 34, pp. 340–345, Mar./Apr. 1998.

[6] J. W. Choi and S. K. Sul, "New compensation strategy reducing voltage/current distortion in PWM VSI systems operating with low output voltages," *IEEE Trans. Ind. Applicat.*, vol. 31, pp. 1001–1008, Sept./Oct. 1995.

**Shaotang Chen** (S'93–M'96–SM'99) received the B.Eng. and M.Eng. degrees from the Central China University of Science and Technology, Wuhan, China, in 1983 and 1986, respectively, and the M.S. and Ph.D. degrees from the University of Wisconsin–Madison, in 1993 and 1995, respectively.

From 1986 to 1991, he was with the Central China University of Science and Technology. From 1995 to 1999, he was a Senior Research Engineer with the Electric and Electronics Department, Research and Development Center, General Motors, Warren, MI. He is currently a Staff Research Engineer with Delphi Research Laboratories, Shelby Township, MI. His current research interests are in control of electric machines, electric machine drives, and power converters.

Dr. Chen was the recipient of a 1999 First Prize Transactions Paper Award presented by the IEEE Industry Applications Society.

**Chandra Namuduri** received the B.Tech degree from the Indian Institute of Technology, Kharagpur, India, in 1981, and the M.Sc. and Ph.D. degrees from Queens University, Kingston, ON, Canada, in 1983 and 1988, respectively, all in electrical engineering.

From December 1985 to March 1989, he was an Electronics Development Engineer with North Hills Electronics, Glen Cove, NY, where he was involved with custom switching power supplies, UPS systems, and dc–dc converters for various industrial applications. From March 1989 to August 1993, he was a Senior Research Engineer with the Research and Development Center, General Motors, Warren, MI, where he was involved in power electronics and motor control schemes for electric and hybrid vehicles. Since August 1993, he has been a Staff Research Engineer with the Research and Development Center, General Motors, where he has been involved with innovative power electronic and electromagnetic systems for automotive applications such as semiactive suspensions, electric power-steering systems, new electrical power system architectures, and fuel economy enhancement techniques. His current research interests are automotive applications of power electronics, smart actuators, and digital control of electromechanical systems.

Dr. Namuduri was the recipient of an IEEE Industry Applications Society (IEEE IAS) Conference Second Best Paper Award.

**Sayeed Mir** was born in Kashmir, India. He received the B.E. degree from the University of Kashmir, Kashmir, India, in 1988, and the M.S. and Ph.D. degrees from the University of Akron, Akron, OH, in 1993 and 1997 respectively, all in electrical engineering.

He currently leads the Power Electronics and Motor Controls Group, Delphi Saginaw Steering Systems, Saginaw, MI, where he is engaged in the development of advance drives for automotive steering application. Prior to joining Delphi Saginaw Steering Systems, he was with the Research and Development Center, General Motors, Warren, MI, from 1997 to 1998. His previous work experience includes power development, Kashmir Government, and summer co-op. with the Thermal Power Station Budarpur, New Delhi, India. His research interest includes power electronics, electric power steering, automotive applications of electric motor drives, modeling and control of electrical machines, adjustable speed drives, control systems applications, fuzzy logic and neural-network application in control systems, DSPs, and microcontrollers.